Multi-objective optimization of district energy systems with demand response

Multi-objective optimization of district energy systems with demand response

Martina Capone[*a)], Elisa Guelpa[a)], and Vittorio Verda[a)]

[a)]*Energy Department, Politecnico di Torino, Corso Duca Degli Abruzzi 24, 10129 Torino, Italy*

[*]Corresponding author: martina.capone@polito.it

Abstract. In district energy applications, implementation of management strategies is crucial to achieve reductions in primary energy consumption and carbon dioxide emissions. The development of optimization tools to upgrade the operation of smart energy systems should take into account all the relevant elements of these complex infrastructures. In this paper, a global optimization approach, applied to district heating, cooling and electricity networks interconnected to each other, is proposed. The suggested approach combines the optimization of the production side, useful to understand how it is convenient to produce heat, cold and electricity, with demand-side management for district heating customers. This is reached by using a bi-level optimization structure, exploiting the genetic algorithm and linear programming. A physical model of the district heating network is included in the procedure to accurately reproduce the effects of demand-side management. The tool can be applied to different objective functions. In this paper, a multi-objective optimization is carried out with two different objective functions: the operation cost and the carbon dioxide emissions. Results show that, by choosing an intermediate trade-off among the two goals, it would be possible to have a 12% reduction in the emissions at the expense of a 25% increase in the operating cost.

Keywords: Vector optimization; energy hub; district heating; thermal network; production optimization; demand-side management.

1. INTRODUCTION

Nowadays, district heating and cooling are convenient solutions to satisfy the thermal and cooling demands of buildings located in high-population density regions. These technologies can guarantee lower carbon dioxide emissions with respect to conventional systems (such as individual boilers and air conditioners), since they mainly exploit energy sources that would otherwise be lost [1].

Until recently, most of the district heating and cooling systems in the world are supplied with combined heat and power plants, which are meant to cover the base load, while heat-only boilers are generally used during the peaks [2,3]. However, in the last few years, the connections among district heating and cooling networks and the other energy grids are becoming increasingly tight. For this reason, a new concept has been coined to refer to interconnected district heating, cooling and electricity grids, and in some cases also to gas networks: the concept of Multi-Energy Systems (MES) [4,5]. The great potential of the interconnections lies in the possibility of converting each form of energy into a different energy vector, when this is convenient; this is done by using energy converters, such as heat pumps or power-to-cool technologies. The convenience is amplified if storage units are installed in the system, since this allows to select the form of energy to be stored [6,7].

The advantages provided by the interconnections of different energy grids, combined with the exploitation of low-grade and sustainable energy sources, allow significant primary energy reductions [8,9]. Thus, district heating and cooling will remain leading-edge technologies for potential emission reduction in the following years, and the increasing interconnection trend will be probably confirmed in the next decades [10].

Within the framework of Multi-Energy Systems, the range of possible operations can be quite wide. The most favorable operation is very often not easily predictable: this may be linked to the wide variety of production layouts, the great interest in exploiting fluctuating renewable sources, the presence of energy conversion technologies and storages and the great variation of consumption and energy prices. For these reasons, optimization models for the operation management

of multi-energy systems are of great interest in the literature. Such models should be able to take into consideration the overall energy system, including the influence of each energy system to the other ones, in order to identify the best solutions [11]. The best solutions are mainly defined in terms of carbon emissions, production costs, revenues, operation and/or investment costs and renewable exploitation [12]. These goals are pursued using different approaches. Wang et al. [13] developed a linear programming (LP) algorithm to optimize the planning of a CHP-DH system with renewables sources and a thermal energy storage. Mixed integer linear programming (MILP) is largely adopted to solve multi-energy production optimization. Bischi et al. [14] faced the problem of the short-term planning of a combined cooling, heat and power (CCHP) energy system by converting the initial MINLP formulation into a MILP using a piecewise linear approximation. A similar problem has been addressed in [15] including the rolling horizon algorithm to take into account the data uncertainty. In [16], [17] MILP has been adopted for both operation and design respectively for a distributed energy system and to supply and industrial area. Finally, non-linear programming (NLP) or Mixed Integer Non-linear programming (MINLP) formulations are mainly used in case the problem is highly non-linear. Powell et al. [18], for example, introduced an algorithm to solve a complex dynamic optimization problem with energy storages by decomposing the original problem into multiple static MINLP problems; other examples of usage of MINLP are [19]–[21].

Despite all the previous works deeply addressed the problem of the optimal energy supply to the consumers, they do not take into account the active role of the consumers as a mean to increase the overall efficiency of an integrated energy system. As stated by Schweiger et al. [22], the consumer represents a key element of any smart energy system. The options for an active participation of the users in the development of an efficient and intelligent energy system are multiple. One of the most interesting is the implementation of Demand Side Management (DSM) actions [23], [24], which can be used to reduce the total energy demand. In particular, short-term demand side actions (i.e. Demand Response) are an effective way to reduce the load peaks and to fill the valleys. In district heating applications, Demand Side Management can be implemented either by applying changes to the heating systems schedules or by adopting a different control strategy [25]. The main purpose is to cut the thermal peaks [26] in order to avoid using low efficiency production units that would decrease the overall efficiency of the system. It represents an excellent alternative to the installation of heat storage tanks to limit the mass-flow rates circulating in the system in order to control the pumping costs and to avoid compromising the possibility of network expansion [27]. Also, the combined adoption of demand response and storages is of great interest. Because of these interesting features, the opportunities for demand-side management in district heating applications have been investigated by various works, such as [28]–[34]. An extensive survey of the different attempts that can be found in literature was presented by [24]. To mention some examples, Basciotti and Schmidt [35] proposed an implementation technique of load shifting that allows peak reductions up to 35%. In [36], DSM was applied to a real district heating network in a multi-scenario simulation analysis and peak reductions in the range from 5% to 35% were obtained depending on the scenario analyzed and on the limitations introduced. Another approach for implementing demand-response in district heating was presented by [37], who chose to prioritize the supply of domestic hot water at the expense of space heating and achieved a decrease in the peak load of about 15% and corresponding energy savings of about 9%.

In this framework, it is essential to incorporate the increasingly central role of the consumers in the development of suitable optimization models. Nevertheless, in the scientific literature, the optimization of multi-energy systems/energy hubs are mainly based on supply-side management strategies. Few researchers have investigated the topic of combined supply and demand-side optimizations and, in most cases, the flexibility of the users was exploited just from the electric network perspective [38], [39]. A first attempt to combine all the aforementioned aspects was done by Reynolds et al. [40] and consists in the development of an optimization strategy which optimizes both the generation and the demand. The optimization was performed on a multi-vector energy system including natural gas, electricity, and heat and modelled the building using EnergyPlus. However, they neglected the influence of the network: the thermal dynamics (such as heat losses, thermal lag and return temperatures) are not taken into account by this study, but they are, as stated by the authors themselves, worthwhile to include in a real-case analysis. The importance of modelling the temperature dynamics of a district heating network is also confirmed by a huge number of papers in literature [41], [42].

The aim of this paper is to propose a tool methodology for the estimation of the optimal operations of a multi-energy system, both from the production and the demand point of view. The system analyzed involves various technologies to produce heat, cold and electricity and various kind of storages (hot, cold and electricity). The energy produced is delivered to customers located in a small district energy system by means of district heating, cooling and electricity infrastructures. Moreover, the possibility of applying demand side management for the thermal network is included and a physical model of the district heating network is used to properly evaluate the effects of load shifting on the thermal dynamics within the network. The main novelties of the paper are:

- the simultaneous optimization of demand and production for a multi-vector energy system, including heat, cold and electricity (this is obtained by means of a bi-level optimization structure where the upper-level optimization, executed by means of a genetic algorithm, is devoted to demand-side management, while the lower-level uses a linear programming algorithm to find the best production layout);

- the consideration of the network behavior by means of a physical model of the district heating network; this model is included in the optimization tool in order to properly evaluate the thermal load at production plant without neglecting the thermal transients in heat transport and distribution;
- the development of a multi-objective optimization tool that allows to examine different and conflicting objective functions (in this specific case-study, the economic aspect and the environmental impact of the system are taken into account).

The paper is structured as follows:

- Section 2: the most important aspects and characteristics of the case-study are discussed;
- Section 3: the methodology used for the optimization is explained;
- Section 4: the most important results of the optimization are reported and discussed;
- Section 5: the main conclusions of this work are outlined.

2. CASE STUDY

The case study analyzed in this paper involves a complex multi-energy system. The system is made up by several end-users, with predetermined needs in terms of heating, cooling and electricity demand. The users are connected to a local production plant by means of an infrastructure including a district heating network (represented in Figure 1), a cooling network and an electricity network.

Different production units are included in the production plant, which has to satisfy the heating, cooling and electricity loads. These are:

- a combined heat and power plant (CHP), which uses natural gas from the national grid to produce heat and electricity;
- a heat-only boiler (HOB), which uses natural gas from the national grid to produce heat;
- a photovoltaic plant (PV), which produces electricity depending on the solar radiation available during the day;
- an electric heat pump (EHP), which absorbs electricity to produce both heat and/or cold;
- an absorption refrigeration unit (ARU), which absorbs thermal power to produce cold;
- an electric storage unit;
- a thermal storage unit;
- a cold storage unit.

Moreover, thanks to the connection with the national electric grid, it is possible to buy and sell electricity from the grid (in this case proper transmission efficiencies are considered). A schematic of the production plant structure is given in Figure 2. The storage units, which are not represented in the scheme, are used to store energy when the production is more convenient; then, the energy is released and used to fulfill the loads when producing is less cost-effective.

Overall, the electricity exchange with the national electric grid and the purchased natural gas are the only resources driving the whole production unit: they are the only elements associated to specific operating costs and CO_2 emissions.

In this analysis, the operation of the system is optimized for a typical winter day, with known cooling demand for industrial buildings, and heating and electricity demands for industrial and residential buildings. Differently from the cooling and electricity loads, which are fixed, the heating demand is supposed to be flexible. Hence, it is possible to apply thermal demand side management to vary the heating demand profile of the customers according to the plant needs.

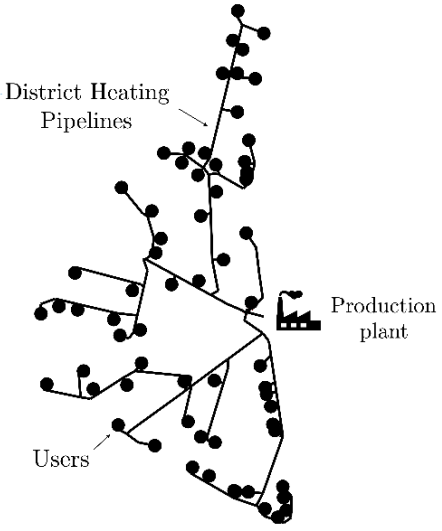

Figure 1 Topology of the district heating network.

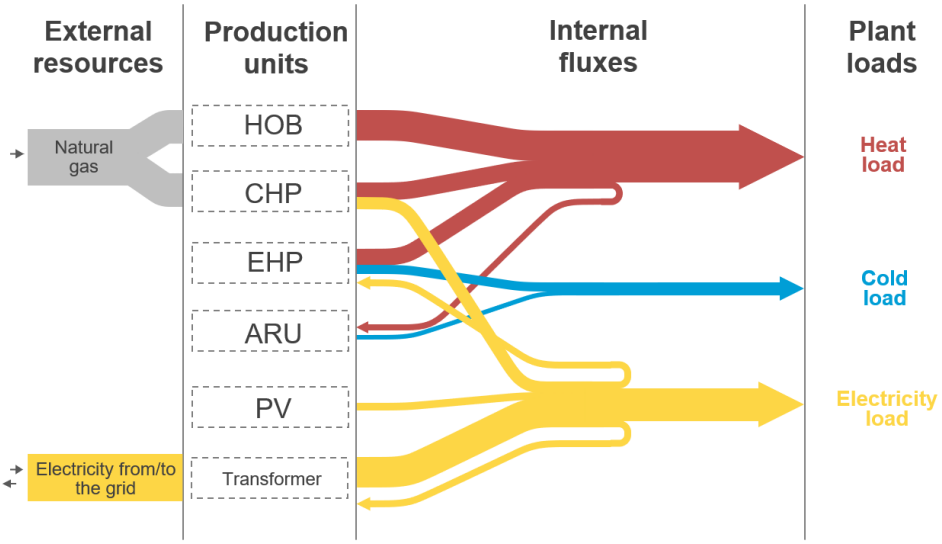

Figure 2. Schematic representation of the production units in the plant. Red, light blue and yellow lines respectively represent the heat, cold and electricity flows. For the sake of simplicity, the storage units are omitted in this scheme.

3. METHODOLOGY

The aim of this paper is to develop a comprehensive optimization tool that combines the optimization of the demand and production of a complex multi-vector energy system and is able to take into consideration the complex thermal dynamics occurring within a district heating network. Due to the different objectives that can be important in this kind of analyses, the optimization should be structured in a multi-objective perspective. To do that, a bi-level optimization structure was used. In this section, the methodology developed to perform the multi-objective optimization is outlined: the optimization model is described starting from its general definition; the different levels of the algorithm are then described in the following subsections.

The multi-objective optimization model developed in this paper is defined by two objective functions: the total operation cost and the carbon footprint of the production system. In mathematical terms, the problem can be formulated as:

$$\min_{\mathbf{x}\in X}(f_{eco}(\mathbf{x}), f_{env}(\mathbf{x})) \tag{1}$$

where the set X is the feasible region of the decision vector $\mathbf{x}$, f_{eco} represents the economical objective function and f_{env} is the environmental objective function. Since f_{eco} and f_{env} can be conflicting, improvements in one of them could deteriorate the other one. In this case, the optimal solution of the multi-objective problem is a set of solutions, which is represented by the so-called Pareto front. Each solution in the Pareto front, which is called Pareto solution $\mathbf{x}_{Pareto}$, represents an optimal solution and satisfies the following condition: there does not exist any other feasible solution $\mathbf{x} \in X$ such that the inequalities $f_{eco}(\mathbf{x}) \leq f_{eco}(\mathbf{x}_{Pareto})$ and $f_{env}(\mathbf{x}) \leq f_{env}(\mathbf{x}_{Pareto})$ are simultaneously verified.

The decision variable vector $\mathbf{x}$ includes all the optimization variables of the problem, i.e. the fluxes involved in the different production units and the variables related to the modification of the customers' thermal profiles (i.e. demand side management). Hence, it can be considered as composed by two different decision variable vectors $\mathbf{p}$ (for the production) and $\mathbf{d}$ (for the demand). The two objective functions f_{eco} and f_{env} are directly dependent on the decision variable vector $\mathbf{p} \in P$, while $\mathbf{d} \in D$ establishes a set of inequality constraints on the production side (depending on the thermal load evolution to be supplied). Consequently, the feasible region of the decision vector $\mathbf{p}$ is $P(\mathbf{d})$ and Eq. (1) can be rewritten in the following form:

$$\min_{\mathbf{p}\in P(\mathbf{d}),\ \mathbf{d}\in D}(f_{eco}(\mathbf{p}), f_{env}(\mathbf{p})) \tag{2}$$

Due to the assumption of constant efficiencies of the generation units, the two objective functions f_{eco} and f_{env} are linear with respect to the production decision vector $\mathbf{p}$. On the other hand, the relationship of P with the demand decision vector

d is nonlinear. In particular, the values of the demand decision vector **d** determine, by means of a non-linear relationship given by a thermo-fluid dynamic model of the district heating network, the evolution of the thermal load at production plant Φ_t, which is used to establish multiple inequality constraints on the production optimization variables **p**. Hence, the feasible domain of the production optimization variables can be expressed as $P(\Phi_t(\mathbf{d}))$. These dependencies will be addressed later on in this section. Therefore, the optimization problem is, on the whole, a nonlinear programming problem (NLP).
In order to exploit the linearities of the problem, it has been decided to decompose it into two different levels: the upper-level deals with the optimization of the demand, which is solved by means of a genetic algorithm, while the lower-level solves the production optimization using a deterministic algorithm suitable for linear programming. As a result, the formulation of the problem becomes:

$$\begin{aligned} &\min_{\mathbf{d}\in D} \quad (f_{eco}(\mathbf{p}), f_{env}(\mathbf{p})) \\ &\text{s.t.} \quad \min_{\mathbf{p}\in P(\Phi_t(\mathbf{d})).} \quad (f_{eco}(\mathbf{p}), f_{env}(\mathbf{p})) \end{aligned} \tag{3}$$

As suggested by Wang et al. [43], the lower-level multi-objective optimization problem has been reformulated as a single-objective optimization problem, with an aggregated objective function obtained using the weighted sum method. In the aggregated objective function, the normalized expressions of f_{eco} and f_{env} appear (respectively f'_{eco} and f'_{env}). The weighting coefficient α (which is bounded between 0 and 1) is automatically handled by the upper-level genetic algorithm. This decomposition brings to a new formulation of the optimization problem, expressed by Eq. (4), in which α is systematically manipulated by the upper-level genetic algorithm and no more adjusted by the lower-level optimization.

$$\begin{aligned} &\min_{\mathbf{d}\in D} \quad (f_{eco}(\mathbf{p}), f_{env}(\mathbf{p})) \\ &\text{s.t.} \quad \min_{\mathbf{p}\in P(\Phi_t(\mathbf{d})).} \quad (\alpha f'_{eco}(\mathbf{p}) + (1-\alpha)\, f'_{env}(\mathbf{p})) \end{aligned} \tag{4}$$

Therefore, at each iteration of the multi-objective upper-level genetic algorithm, which is used to find the optimal set of demand side variables, a single-objective lower-level deterministic optimization is carried out to optimize the variables related to the production plant. Moreover, a simulation of the thermo-fluid dynamic behavior of the district heating network is needed at each iteration to evaluate Φ_t in order to determine the search space of the production optimization variables.
The approach developed in this paper can be used also when more objective functions are considered. In this case, the problem formulation can be written as follows:

$$\begin{aligned} &\min_{\mathbf{d}\in D} \quad (f_1(\mathbf{p}), \dots, f_k(\mathbf{p})) \\ &\text{s.t.} \quad \min_{\mathbf{p}\in P(\Phi_t(\mathbf{d})).} \quad \textstyle\sum_k (w_k f'_k(\mathbf{p})) \end{aligned}$$

where w_k are the weighting factors, handled by the upper-level optimizer and defined such that $\sum_k w_k = 1$.
A synthesis of the bi-level multi-objective optimization approach is reported in the flowchart in Figure 3. The different steps are discussed in the next subsections.

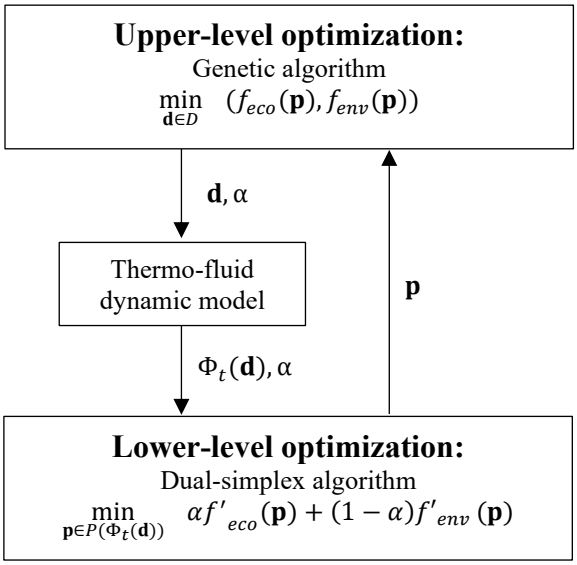

Figure 3 Flowchart of the bi-level multi-objective optimization algorithm

3.1 Upper-level optimization: demand-side management

In order to evaluate the total operation cost and the daily carbon emission for the system considered, it is needed to know the evolution of the thermal, cold and electricity loads during the day. In this analysis, the cold and electricity loads at plant level were supposed to be known in advance and fixed. As concerns the thermal load, it was assumed as flexible. In particular, it was hypothesized that the expected thermal request of each user can be subjected to anticipations up to 30 minutes. This limitation was introduced to avoid undermining the thermal comfort of the users. Moreover, for technical reasons, anticipations were allowed to be operated every 5 minutes (e.g. 5 min, 10 min, 15 min etc. up to 30 min).
The anticipation time of the buildings were used as independent variables for the demand-side management optimization. They were included in the decision vector **d**, having so many elements as the number of buildings connected to district heating (58 in the case-study considered). Each decision variable d_i is related to the anticipation time of the i-th building Δt_i according to the following relationship:

$$\Delta t_i = 5\ [min] \cdot d_i$$

d_i can only assume an integer value and is bounded below by 0 (no anticipation, $\Delta t_i = 0\ min$) and above by 6 (maximum anticipation allowed, $\Delta t_i = 30\ min$).
To relate anticipations with the thermal load at plant level, the solution of the whole thermo-fluid dynamic problem in the district heating network is required. Then, once all the energy loads at plant level are known, the use of a tool for production optimization is recommended to obtain proper input flows for the different technologies in order to minimize the objective function considered. Therefore, the problem formulation turns out to be mixed-integer nonlinear.
The genetic algorithm (GA) was adopted to solve the upper-level optimization of this complex MINLP problem. This choice was motivated by the successful results obtained by numerous works using GA for DSM applications, since it allows to easily manage MINLP formulations and avoids the risk of getting stuck to local minima [24], [40]. The Global Optimization Toolbox of MATLAB was used for this purpose.

3.2 Thermo-fluid dynamic model

A suitable physical model is needed to evaluate the thermal load at plant level once the thermal profiles of the buildings are known. Differently from the electricity and cooling loads, the heating load at plant level is not fixed throughout the optimization procedure, due to the possibility of performing thermal demand side management. For this reason, the behavior of the district heating network was simulated at each iteration of the genetic algorithm.
In this study, a one-dimensional thermo-fluid dynamic model was adopted. The complex structure of the network was described by means of the graph theory [44]: each pipe was treated as a branch starting from a node, which corresponds to the inlet section, and ending in another node, which is the outlet section. The topology of the network was taken into account within the incidence matrix **A**, which has as many rows as the number of nodes, NN, and as many columns as the number of branches, NB. Each element of the incidence matrix A_{ij} is equal to 1 if the i-th node is the inlet node of the j-th branch, -1 if it is the outlet node, and 0 if the i-th node and the j-th branch are not related to each other.
The model, which was applied to both the supply and return lines of the district heating network, is based on the conservation equations of mass, momentum and energy, which are reported in Eqs. (5-7)

$$\frac{\partial \rho}{\partial t} + \frac{\partial (\rho u)}{\partial x} = 0 \tag{5}$$

$$\rho \frac{\partial u}{\partial t} + \rho u \frac{\partial u}{\partial x} = -\frac{\partial p}{\partial x} - F_{FRICT} + F_1 \tag{6}$$

$$\frac{\partial (\rho c_p T)}{\partial t} + \frac{\partial (\rho c_p u\, T)}{\partial x} + \varphi_{loss} = 0 \tag{7}$$

where F_{FRICT} takes into account the viscous forces, F_1 represents the source term accounting for the effect of local fluid dynamic resistance due to valves or junctions and the effects of pressure rise due to pumps, and φ_{loss} accounts for the thermal losses. Regarding Eq. (7) it is worth to mention that the conductive term was neglected.
The model was considered in a pseudo-dynamic form: the hydraulic problem, composed of Eq. (5) and Eq. (6), was approximated as steady-state because of the rapidity of the fluid-dynamic perturbations, which reach the whole network in a period of time of few seconds, while the energy equation, Eq. (7), was solved dynamically, because temperature perturbations travel at the fluid velocity and could take a long time to be propagated within the network.

The conservation equations were integrated according to the finite volume method [45]. More in detail, the continuity and energy equations were integrated over control volumes including each junction node and half of the branches entering or exiting that node. As concerns the momentum equation, control volumes including each branch with the two delimiting nodes were considered. The integrated form of the conservation equations is the following:

$$\mathbf{A} \cdot \mathbf{G} + \mathbf{G_{ext}} = \mathbf{0} \tag{8}$$

$$\mathbf{G} = \mathbf{Y} \cdot \mathbf{A^T} \cdot \mathbf{P} + \mathbf{Y} \cdot \boldsymbol{\tau} \tag{9}$$

$$\mathbf{M} \cdot \dot{\mathbf{T}} + \mathbf{K} \cdot \mathbf{T} = \mathbf{g} \tag{10}$$

where arrays **G** (length: *NB*), **P** (length: *NN*), and **T** (length: *NN*) are the unknowns of the problem, containing respectively the mass flow rates in each branch and the pressures and temperatures in each node of the system. The other terms are: the abovementioned incidence matrix **A** (size: *NN* × *NB*); array $\mathbf{G_{ext}}$ (length: *NN*), which contains the mass flow rates injected in or extracted from the system; fluid dynamic conductance matrix **Y** (size: *NB* × *NB*), accounting for the pressure losses; vector $\boldsymbol{\tau}$ (length: *NB*), which represents the pressure rise due to pumps; the mass matrix **M** (size: *NN* × *NN*); the stiffness matrix **K** (size: *NN* × *NN*); the known terms vector $\boldsymbol{g}$ (length: *NN*).
The interested reader is referred to Sciacovelli et al. [46] for a detailed description of the algorithm used for the solution of this thermo-fluid dynamic problem. In the case of a three-shaped network, mass-flow rates can be easily computed from the solution of Eq. (8), since they are independent from the pressure distribution within the network. For this reason, Eq. (9) was ignored in this analysis. A diagram including the resolution method adopted and the boundary conditions provided to the algorithm is reported in Figure 4. The whole procedure was implemented within the MATLAB® environment; in order to solve the linear systems, the function *mldivide* was used. The simulation time step used for the simulation is $5\ min$. The network problem was solved at each iteration of the genetic algorithm due to the different thermal request of the users. The solution allowed an accurate estimation of the thermal load at plant level $\Phi_{t,plant}$, which was evaluated as:

$$\Phi_{t,plant}(t) = G_{plant}(t) c_p (T_{p,supply} - T_{p,return}(t)) \tag{11}$$

where the total mass-flow rate G_{plant} and the return temperature at the production plant $T_{p,return}$ are outputs of the model. Validation of the one-dimensional thermo-fluid dynamic model described in this paragraph can be found in previous works [34], [47].

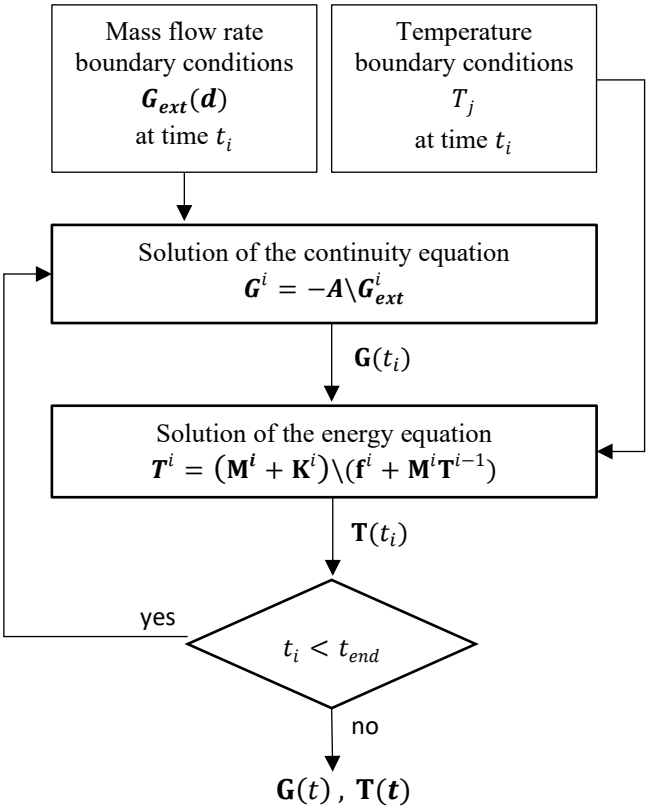

Figure 4. Schematic of the algorithm adopted for the solution of the thermo-fluid dynamic problem.

3.3 Lower-level optimization: production optimization

The last step of the optimization tool presented in this paper consists in optimizing the thermal, cold and power fluxes within the production plant. The goal is to effectively distribute the production among the available components so that

the daily operation costs or the carbon emissions are minimized. This is possible only once the thermal, cold, and electric loads are known. Consequently, this step is subsequent to the thermo-fluid dynamic simulation of the district heating network, needed to properly evaluate the thermal load at plant level.
The objective function considered in this lower-level optimization was an aggregate of the economic objective function, expressed by Eq. (12), and the environmental objective function, expressed by Eq. (13).

$$f_{eco} = \sum_{i=1}^{N_{TS}} \left(c_g (\Phi_{g,CHP}^i + \Phi_{g,HOB}^i) + c_{e,in}^i \Phi_{e,in}^i - c_{e,out}^i \Phi_{e,out}^i \right) \Delta t_s \tag{12}$$

$$f_{env} = \sum_{i=1}^{N_{TS}} \left(e_g (\Phi_{g,CHP}^i + \Phi_{g,HOB}^i) + e_e (\Phi_{e,in}^i - \Phi_{e,out}^i) \right) \Delta t_s \tag{13}$$

As suggested by the expressions, the economic objective function and the environmental objective function are represented by the sum of, respectively, the operating costs and the emissions in each time interval i of the day, which is divided into a number of time steps N_{TS} equal to 96, each one equal to $\Delta t_s = 15\ min$.
The economic objective function is represented by the daily operating cost. The expenses for the operation of the plant are due to the amount of natural gas consumed by the cogeneration and the boiler units and to the electricity purchased from the grid, while revenues are available if electricity is sold. The specific cost of the natural gas c_g was supposed to be constant. In contrast, the specific costs of the electricity purchased ($c_{e,in}^i$) or sold ($c_{e,out}^i$) to the grid vary in time.
The same applies for the environmental objective function. CO_2 emissions are due to the natural gas burned by the cogeneration and the boiler units and to the electricity purchased from the grid. Coherently, the electricity sold to the grid was considered as a revenue. In this case, the specific emission coefficients (e_g for natural gas and e_e for electricity) were all assumed constant during the day. With regard to the emission coefficient for the external electricity production e_e, the value to disposition from ISPRA [48] for Italy was used.
As previously explained, the two objective functions were combined by means of the following relationship:

$$OF = \alpha f'_{eco} + (1 - \alpha)\, f'_{env} \tag{14}$$

where OF represents the aggregated objective function and α is the weighting coefficient, bounded between 0 and 1. The economic and environmental objective functions have been normalized according to the following relationships:

$$f'_{eco} = \frac{f_{eco} - \min f_{eco}}{\max f_{eco} - \min f_{eco}}$$

$$f'_{env} = \frac{f_{env} - \min f_{env}}{\max f_{env} - \min f_{env}}$$

The two objective functions (and, as a consequence, the aggregated objective function) are linearly dependent on:

1. the natural gas required for the operation of the cogeneration unit $\Phi_{g,CHP}^i$;
2. the natural gas required for the operation of the heat-only boiler $\Phi_{g,HOB}^i$;
3. the electric power purchased from the grid $\Phi_{e,in}^i$;
4. the electric power sold to the grid $\Phi_{e,out}^i$,

each one considered as an average value during the i-th time step (with $i = 1{:}\,N_{TS}$). These are the independent variables of the problem, which were obtained as an output of the lower-level optimization problem, along with other decision variables:

5. the electric power needed by the electric heat pump to produce heat Φ_{e,EHP_T}^i;
6. the electric power needed by the electric heat pump to produce cold Φ_{e,EHP_C}^i;
7. the heat required by the absorption heat pump $\Phi_{t,ARU}^i$;
8. the heat absorbed or released by the thermal storage $\Phi_{t,st}^i$;
9. the cooling power absorbed or released by the cold storage $\Phi_{c,st}^i$;
10. the electricity absorbed or released by the electric storage $\Phi_{e,st}^i$.

Because of the storage tanks installed in the system, it was not possible to solve the production optimization independently at each time step. Hence, the operation optimization was solved by considering as decision variables the 10 above-mentioned flows for each time step i, with $i = 1{:}\,N_{TS}$. Since N_{TS} is equal to 96, the total number of decision variables in a day for the production optimization part, included in the array $\mathbf{p}$, is 960:

$$\mathbf{p}_{10\mathrm{N_{TS}}\times 1} = [\Phi_{g,CHP}^1 \ \ \Phi_{g,HOB}^1 \ \ \Phi_{e,in}^1 \ \ \Phi_{e,out}^1 \ \ \Phi_{e,EHP_T}^1 \ \ \Phi_{e,EHP_C}^1 \ \ \Phi_{t,ARU}^1 \ \ \Phi_{t,st}^1 \ \ \Phi_{c,st}^1 \ \ \Phi_{e,st}^1$$
$$\Phi_{g,CHP}^2 \ \ \Phi_{g,HOB}^2 \ \ \Phi_{e,in}^2 \ \ \Phi_{e,out}^2 \ \ \Phi_{e,EHP_T}^2 \ \ \Phi_{e,EHP_C}^2 \ \ \Phi_{t,ARU}^2 \ \ \Phi_{t,st}^2 \ \ \Phi_{c,st}^2 \ \ \Phi_{e,st}^2 \ \cdots \tag{15}$$

$$\cdots \Phi_{g,CHP}^{N_{TS}} \quad \Phi_{g,HOB}^{N_{TS}} \quad \Phi_{e,in}^{N_{TS}} \quad \Phi_{e,out}^{N_{TS}} \quad \Phi_{e,EHP_T}^{N_{TS}} \quad \Phi_{e,EHP_C}^{N_{TS}} \quad \Phi_{t,ARU}^{N_{TS}} \quad \Phi_{t,st}^{N_{TS}} \quad \Phi_{c,st}^{N_{TS}} \quad \Phi_{e,st}^{N_{TS}} \,]^{\mathrm{T}}$$

All the variables are continuous. Their lower and upper bounds (contained in the vectors $\mathbf{l_b}$ and $\mathbf{u_b}$) are reported in Table 1. Except for the storage flows, which assume negative values when the charging process occurs, all the other variables are bounded from below by zero. The upper bounds, instead, correspond to the maximum power that each component can provide, depending on its size. The variables $\Phi_{e,in}^{i}$ and $\Phi_{e,out}^{i}$, representing the electricity purchased and sold to the grid, are not bounded from above: they can assume any positive value.

Table 1. Upper and lower bounds for the design variables of the lower-level production optimization.

Design variable	Lower bound	Upper bound
$\boldsymbol{\Phi_{g,CHP}^{i}}$	$0\ kW$	$4000\ kW$
$\boldsymbol{\Phi_{g,HOB}^{i}}$	$0\ kW$	$4000\ kW$
$\boldsymbol{\Phi_{e,in}^{i}}$	$0\ kW$	$-$
$\boldsymbol{\Phi_{e,out}^{i}}$	$0\ kW$	$-$
$\boldsymbol{\Phi_{e,EHP_T}^{i}}$	$0\ kW$	$500\ kW$
$\boldsymbol{\Phi_{e,EHP_C}^{i}}$	$0\ kW$	$200\ kW$
$\boldsymbol{\Phi_{t,ARU}^{i}}$	$0\ kW$	$600\ kW$
$\boldsymbol{\Phi_{t,st}^{i}}$	$-600\ kW$	$600\ kW$
$\boldsymbol{\Phi_{c,st}^{i}}$	$-400\ kW$	$400\ kW$
$\boldsymbol{\Phi_{e,st}^{i}}$	$-1000\ kW$	$1000\ kW$

Moreover, the design variables need to satisfy 9 inequality constraints for each time step. The first three inequality constraints are related to the thermal, cooling and electricity balance. At each time step $i = 1{:}\,N_{TS}$ and for each energy vector $j = 1{:}\,3$ (heat, cool and electricity), the following condition must be satisfied: $production_j^i \geq consumption_j^i$. This means that production must be greater than consumption at any time and for each energy vector. Note that the inequality arises from the possibility to dissipate heat, cold and electricity.

In the described system, the thermal production is carried out by means of the heat-only boiler, the cogeneration unit and the electric heat pump. At each time step i, a thermal power equal to $\Phi_{t,HOB}^{i}$, $\Phi_{t,CHP}^{i}$ and Φ_{t,EHP_T}^{i} is respectively delivered by each one of these units. Instead, the thermal consumption is due to the absorption refrigeration unit, whose required heat $\Phi_{t,ARU}^{i}$ is a design variable, and to the users' thermal load Φ_{t}^{i}, which is equal to $\Phi_{t}^{i} = \Phi_{t,plant}(i)$ and is obtained using the thermo-fluid dynamic model of the district heating network. The thermal load is constant at each lower-level optimization step, since it just depends on the demand-side management part and on the decision vector $\mathbf{d}$, which was addressed by the upper-level optimization. Finally, the thermal storage can absorb or produce thermal power: in the charging phase $\Phi_{t,st}^{i} < 0$, while in the discharging phase $\Phi_{t,st}^{i} > 0$. If $\Phi_{t,st}^{i} = 0$ the thermal storage is not used. Hence, the thermal balance for each one of the time steps of the simulation reads as follows:

$$\Phi_{t,HOB}^{i} + \Phi_{t,CHP}^{i} + \Phi_{t,EHP_T}^{i} + \Phi_{t,st}^{i} \geq \Phi_{t,ARU}^{i} + \Phi_{t}^{i} \tag{16}$$

Regarding the cooling balance, the units devoted to the production are the electric heat pump and the absorption refrigeration unit. The cooling power delivered by these units is labelled as Φ_{c,EHP_C}^{i} and $\Phi_{c,ARU}^{i}$. The cooling consumption is only due to the cooling load attributed to the users Φ_{c}^{i}. As for the thermal storage, the cold storage can produce or consume cooling power $\Phi_{c.st}^{i}$ depending on its sign. In view of these considerations, the cooling balance can be written in the following form:

$$\Phi_{c,EHP_C}^{i} + \Phi_{c,ARU}^{i} + \Phi_{c,st}^{i} \geq \Phi_{c}^{i} \tag{17}$$

Finally, electricity is produced by the cogeneration unit and by the photovoltaic system. Moreover, it can be purchased from the external grid. These units respectively supply at each time step a power equal to $\Phi^i_{e,CHP}$, $\Phi^i_{e,PV}$ and $\Phi^i_{e,in'}$. As far as Φ^i_{PV} is concerned, this quantity is supposed to be known in advance, depending on the solar radiation forecast available. Regarding the electricity consumption, electric power is absorbed by the electric heat pump for heat and cold production (Φ^i_{e,EHP_T} and Φ^i_{e,EHP_C}) and by the electricity required by the users Φ^i_e. Also, some electric power $\Phi^i_{e,out'}$ can be sold to the external grid. The electric power absorbed or released by the electric storage is $\Phi^i_{e,st}$. Thus, the electricity balance at each time step is as follows:

$$\Phi^i_{e,CHP} + \Phi^i_{e,PV} + \Phi^i_{e,in'} + \Phi^i_{e,st} \geq \Phi^i_{e,EHP_T} + \Phi^i_{e,EHP_C} + \Phi^i_e + \Phi^i_{e,out'} \tag{18}$$

In order to relate the thermal, cold and electricity balances to the independent variables of the optimization problem, the output power of each production unit needs to be expressed as a function of the input power. Because of the low capacity of the technologies considered in this work, the efficiencies and coefficients of performance (COP) can be considered as constant with a good level of approximation. The following relationships were used:

$$\Phi^i_{t,HOB} = \eta_{HOB}\Phi^i_{g,HOB} \tag{19}$$
$$\Phi^i_{t,CHP} = \eta_{CHP_T}\Phi^i_{g,CHP} \tag{20}$$
$$\Phi^i_{e,CHP} = \eta_{CHP_E}\Phi^i_{g,CHP} \tag{21}$$
$$\Phi^i_{t,EHP_T} = COP_{EHP_T}\Phi^i_{e,EHP_T} \tag{22}$$
$$\Phi^i_{c,EHP_C} = COP_{EHP_C}\Phi^i_{e,EHP_C} \tag{23}$$
$$\Phi^i_{c,ARU} = \eta_{ARU}\Phi^i_{t,ARU} \tag{24}$$
$$\Phi^i_{e,in'} = \eta_{tr}\Phi^i_{e,in} \tag{25}$$
$$\Phi^i_{e,out} = \eta_{tr}\Phi^i_{e,out'} \tag{26}$$

By substituting Eqs. (19-26), the balances become:

$$\eta_{HOB}\Phi^i_{g,HOB} + \eta_{CHP_T}\Phi^i_{g,CHP} + COP_{EHP_T}\Phi^i_{e,EHP_T} + \Phi^i_{t,st} \geq \Phi^i_{t,ARU} + \Phi^i_t \tag{27}$$

$$COP_{EHP_C}\Phi^i_{e,EHP_C} + \eta_{ARU}\Phi^i_{t,ARU} + \Phi^i_{c,st} \geq \Phi^i_c \tag{28}$$

$$\eta_{CHP_E}\Phi^i_{g,CHP} + \Phi^i_{e,PV} + \eta_{tr}\Phi^i_{e,in} + \Phi^i_{e,st} \geq \Phi^i_{e,EHP_T} + \Phi^i_{e,EHP_C} + \Phi^i_e + \frac{\Phi^i_{e,out}}{\eta_{tr}} \tag{29}$$

Besides the energy balance, six more inequality constraints for each time step i are added to take into account the operation of the storage systems within the production plant. For each of the three storages, two constraints are required at each time step. The former is linked with the maximum energy that each storage is able to deliver, which depends on the energy stored in the previous time steps:

$$\int_0^{t_i} \Phi_{t,st}(t)dt \leq 0 \tag{30}$$
$$\int_0^{t_i} \Phi_{c,st}(t)dt \leq 0 \tag{31}$$
$$\int_0^{t_i} \Phi_{e,st}(t)dt \leq 0 \tag{32}$$

Instead, the latter is related with the maximum energy that each unit can store, depending on its capacity. The capacities of the thermal, cold and electricity storages, labelled as C_t, C_c and C_e, are respectively 1600 kWh_t, 1200 kWh_c and 5000 kWh_e. All the storages were considered as ideal: the power losses were not taken into account.

$$\left| \int_0^{t_i} \Phi_{t,st}(t)dt \right| \leq C_t \tag{33}$$
$$\left| \int_0^{t_i} \Phi_{c,st}(t)dt \right| \leq C_c \tag{34}$$

$$\left| \int_0^{t_i} \Phi_{e,st}(t)dt \right| \leq C_e \tag{35}$$

The nine expressions reported in Eqs. (27-35) considered for each time step $i = 1{:}\,N_{T_S}$ can be summarized using the following inequality constraint:

$$\mathbf{A_{IC}}\,\mathbf{p} \leq \mathbf{b_{IC}} \tag{36}$$

where $\mathbf{p}$ is the decision variable of the lower level optimization, devoted to production optimization, $\mathbf{A_{IC}}$ is a known matrix of coefficients (of dimensions $9N_{T_S} \times 10N_{T_S}$, since 9 is the number of inequality constraints for each time step and 10 the number of decision variables for each time step) and $\mathbf{b_{IC}}$ is a vector of known coefficients ($9N_{T_S} \times 1$).
To sum up, the lower-level optimization consists in a linear programming problem, which can be written in the form:

$$\begin{array}{ll} \text{Minimize} & \mathbf{c^T p} \\ \text{subject to} & \mathbf{A_{IC}}\,\mathbf{p} \leq \mathbf{b_{IC}} \\ \text{and} & \mathbf{l_b} \leq \mathbf{p} \leq \mathbf{u_b} \end{array}$$

where the vector $\mathbf{c}$ takes into account the combination of specific costs and emissions associated with each variable.
This linear programming optimization problem was solved (at each iteration of the upper-level genetic algorithm) using the dual simplex method, through the MATLAB Optimization Toolbox function *linprog*. Finally, at each iteration, the solution $\mathbf{p}$ was used to evaluate, f_{eco} and f_{env}.

4. RESULTS AND DISCUSSION

The proposed approach was applied to the case-study described in Section 2. The results of the multi-objective optimization are reported and discussed in this section.
The non-optimized configuration is presented beforehand. In Figure 5, the non-optimized thermal load at production plant (obtained without demand side management actions) is reported, together with the cooling load and the electricity load, which remain the same throughout the optimization. This configuration involves thermal, cold and power peaks of respectively 7.6 MW, 0.4 MW and 3.5 MW.

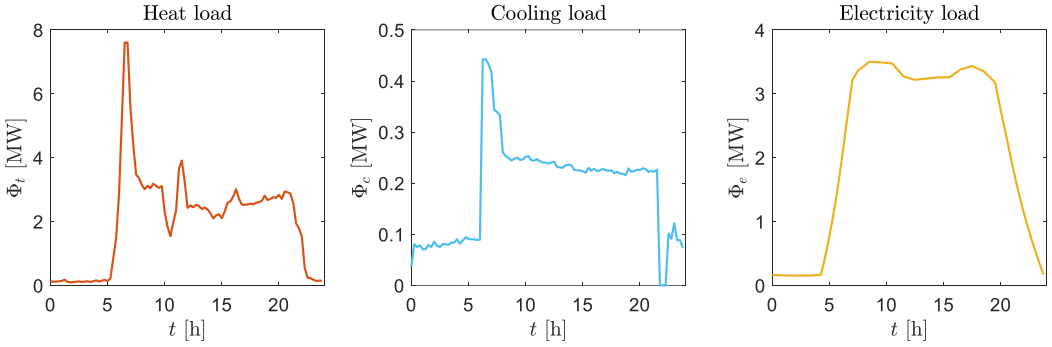

Figure 5. Heat load (non-optimized case), cooling load and electricity load of the district energy system at plant level during a typical winter day.

4.1 Economic optimization

A pure economic optimization was carried out as first step. The optimized profile of the thermal load at plant level is represented and compared to the non-optimized case in Figure 6. The economic optimization allows a significant modification of the heat load at production plant, by applying load shifting to 28 users out of 58. The thermal load is reduced up to 5.3 MW, which is reduced of 30.2% with respect to the non-optimized configuration.
The optimized configuration of the production plant was computed by means of the linear programming optimizer, considering the total daily cost – reported in Eq. (12) – as objective function. The resulting optimal solution is illustrated in Figure 7, where production and consumption of heat, cold and electricity are represented separately. From the analysis of the figure, it is possible to notice that the heat demand, including the thermal needs of the absorption refrigerator, is mainly satisfied using the combined heat and power plant and the heat-only boiler. The electric heat pump is used just

once, when the electric demand is low. The thermal storage is used, when possible, to shift the production in more convenient instants. Concerning cooling, it is almost exclusively supplied by the absorption refrigeration unit, except for a time step in which the electric heat pump is active. Even in this case, the storage is used to shift the cooling production in order to avoid tightening up the heat consumption when the thermal load is high. Finally, the electricity demand, including the consumptions for the electric heat pump (which are actually negligible), is covered with the photovoltaic system, when available, and then with the combined heat and power unit and the electric power purchased from the external grid. A massive usage of the electric storage helps managing with the variable cost of grid's electricity.
This demand side management setup, combined with the afore-mentioned layout of the production plant, guarantees a total daily cost of 4742 €. With this configuration, the corresponding carbon dioxide emissions would be of 24971 kg_{CO2}/day. A comparison can be performed with the results of an economic optimization without demand-side management (production optimization only). In this case, the total daily cost would have been equal to 4840 €, whereas in absence of production optimization the generation units are switched on according to a priority order (and without storage units) leading to a daily operation cost of 5790 €. This means that the production optimization allows a 16.4% reduction in the cost with respect to the non-optimized case, while the combination with demand-side increases the savings of a further 1.7%.

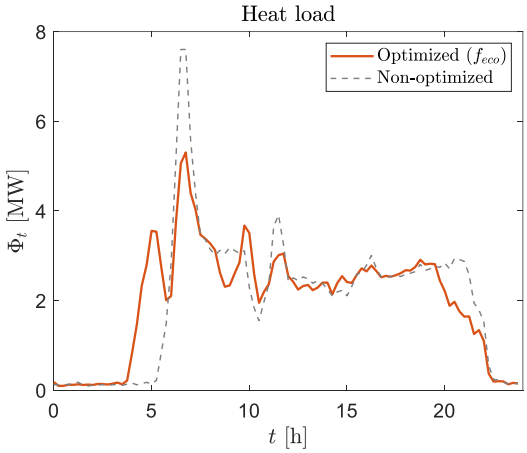

Figure 6. Evolution of the heat load at production plant during the day: comparison of the non-optimized case with the configuration obtained with the economic optimization.

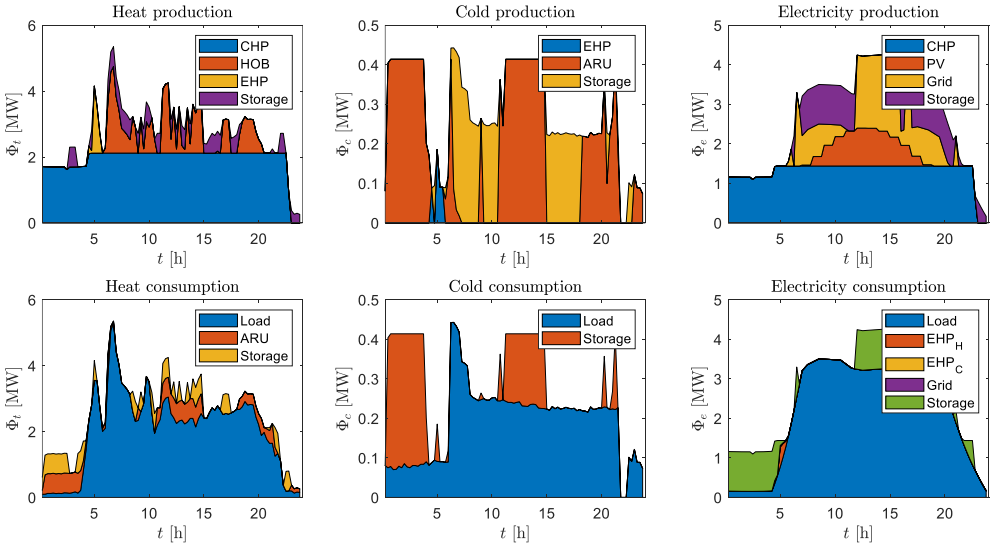

Figure 7. Optimized operation of the production plant resulting from the economic optimization.

4.2 Environmental optimization

As a second step of the analysis, the environmental optimization was performed. The optimization results suggest applying modifications on the demand-side to 33 users out to 58. These modifications bring to a different thermal load at production plant, as illustrated in Figure 8. This profile is slightly different from the one obtained with the economic

optimization. In this case, the thermal peak amounts to 5.0 MW, which corresponds to a reduction of about 34.5% with respect to the base case.
The resulting configuration of the production plant, which was obtained using the environmental objective function described by Eq. (13), is reported in Figure 9. Differently from the previous case, the heat demand is mainly supplied with the electric heat-pump, while the combined heat and power unit is used only when the request exceeds the heat pump capacity. The heat-only boiler is never operated. The heat pump is used also for cooling purposes, instead of the absorption refrigeration unit, which was adopted in the case of the economic optimization. The heat and cold storages are used to partially shift the demand to more convenient time for the electricity production. Concerning the electricity, the demand, including the electric load and the consumptions of the electric heat pumps, is satisfied by the photovoltaic system (when the solar radiation is available), the combined heat and power unit (when it is turned on because of the thermal demand) and the electricity purchased from the grid. The electric storage is used to avoid purchasing from the grid when the price is high.
The main differences with respect to the economic optimization are the greater usage of electricity purchased from the external grid, even for heating and cooling purposes. The electric heat pump turns out to be, from an environmental point of view, a better option than the combined heat and power unit, the boiler, and the absorption refrigeration unit. This is due to the greater efficiency of the external electricity production system with respect to the system considered in this case study.
The value of the environmental objective function obtained with these settings is of about 19826 kg_{CO2}/day. Instead, the economic counterpart is 9638 €/day.
As in the previous case, the results can be compared to the ones provided by production optimization only (without demand-side management) and by the implementation of a priority order for the selection of the production units. These two strategies respectively lead to about 20130 kg_{CO2}/day and 20300 kg_{CO2}/day. Thus, considering the emissions, the percentage reduction guaranteed by the production optimization and by the presence of the storages is only 0.8%, while the combination of demand and production optimization allows a 2.3% reduction in the carbon dioxide emissions (i.e. 1.5% more with respect to production optimization only).

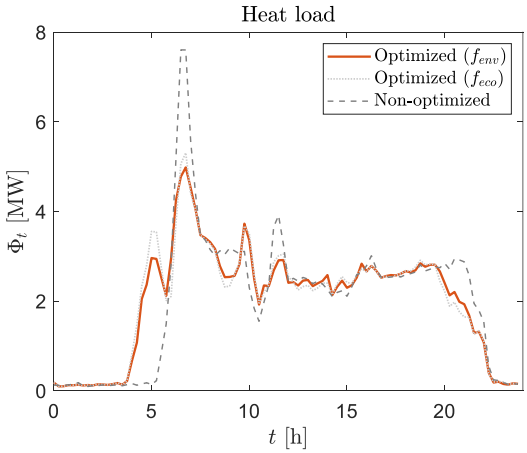

Figure 8. Evolution of the heat load at production plant during the day: comparison of the non-optimized case with the configuration obtained with the economic optimization and with the environmental optimization.

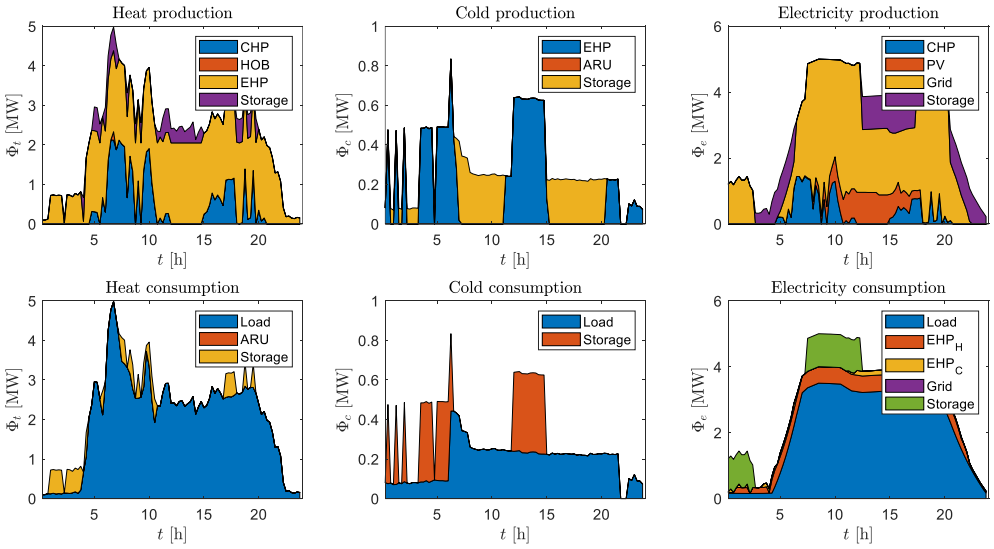

Figure 9. Optimized operation of the production plant resulting from the environmental optimization.

4.3 Multi-objective optimization

Finally, due to the conflicting nature of the two solutions obtained with the economic optimization and the environmental optimization, a multi-objective optimization was carried out – following the methodology developed in Section 2 – in order to identify the whole set of Pareto solutions of the problem.

The Pareto curve is reported in Figure 10. The results of the two single-variable optimizations are highlighted in blue and green, while the grey circles represent the intermediate optimal solutions: as the weighting factor α increases, the multi-objective optimization assigns a larger weight to the economic objective function with respect to the environmental objective function; as a consequence, f_{eco} decreases and f_{env} increases. Regarding the peak reduction, they vary in a range between 29.4% and 40.2%, with respect to the case without demand-side management. Since various papers have analyzed the potential of demand-side management in thermal networks, these results can be compared to other works in the literature. The average value in the present work is 34.4%. This is in line with the results obtained by other DSM studies that reported peak reductions up to 35% depending on the external conditions [35], [36].

The discontinuity in some areas of the Pareto front can be associated to the upper limits of certain production units (related to their size). This can be noticed observing the values assumed by the production variables, reported in Figure 11. In this figure, the energy delivered by each production unit of the plant (calculated as the time integral of the thermal/cold/electricity power of each unit over the whole day) is represented along the whole Pareto front. The following conclusions can be drawn:

- On the thermal side, a greater usage of the electric heat pump increases the production cost, but it helps cutting down the carbon emissions. When the optimization privileges the environmental impact of the production system, at a certain point the electric heat pump reaches its maximum power: in this case, the combined heat and power unit is used to satisfy the reminder of the thermal demand. On the other hand, the combined heat and power unit is preferred in case of greater values of α due to its low costs of production. When this unit reaches its maximum power, the remaining heat demand is supplied either by the heat-only boiler (if more weight is given to the total cost) or by the electric heat pump (if more weight is given to the emissions value).
- On the cooling side, the production is performed either with the electric heat pump (environmental optimization) or with the absorption refrigeration unit (economic optimization). In a certain interval of the Pareto curve, both the cooling production units are used, depending on their convenience in different instants of time.
- Finally, concerning the electricity production, the photovoltaic energy is always totally used. The choice between using the combined heat and power unit or purchasing electricity of the grid depends on the weight assigned to each objective function, following a similar reasoning as in the thermal case.

For a better understanding of the graph, it is worth remembering that all the production units are related to each other. Hence, the behavior of each of them has an influence on the whole system.

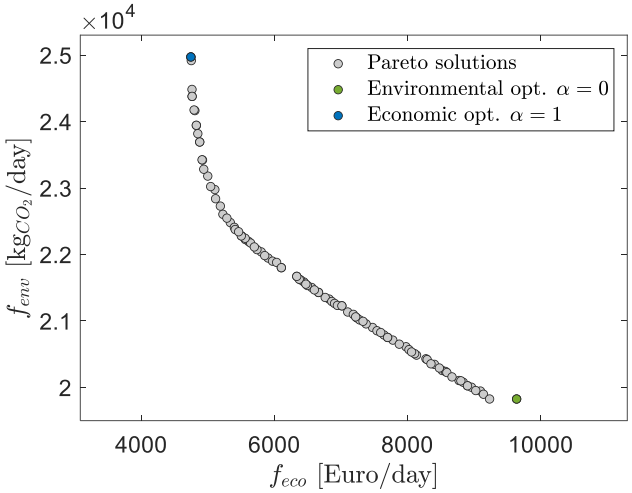

Figure 10. Result of the multi-objective optimization: the Pareto front.

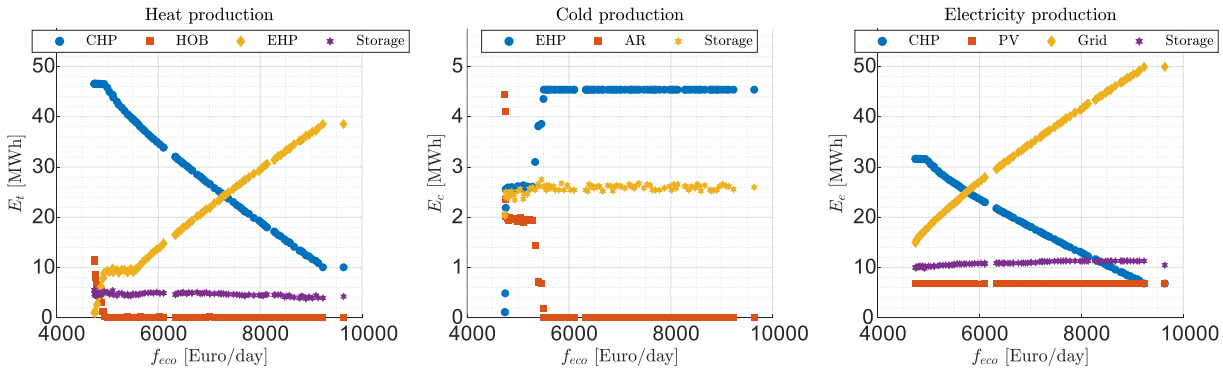

Figure 11. Variation of the energy production along the Pareto curve.

A trade-off between economic and environmental benefits is selected among the Pareto front solutions and this is described in the current section. The optimal solution analyzed brings to a total cost of 5560 €/day and to carbon dioxide emissions equal to 22226 kg$_{CO2}$/day. The weighting factor is approximately equal to 0.48. The thermal load at production plant for the trade-off case is reported in Figure 12. In this configuration the thermal request of 50 users out of 58 are shifted. This allows a reduction of the thermal peak up to 4.8 MW (-37% with respect to the non-optimized case).
The corresponding layout of the production plant is illustrated in Figure 13. In this case, the thermal production is mainly performed with the cogeneration unit; when this is not sufficient to cover the whole thermal demand, the electric heat pump is used. Cold is produced by means of the electric heat pump. Finally, regarding electricity, it is produced by the photovoltaic system and the cogeneration unit; when these units reach their limits, electricity is purchased from the grid. The aforementioned solution is be identified in the curve represented in Figure 14, by an orange point.
The aim of Figure 13 is to report the variation introduced by each Pareto solution with respect to the solution provided by a pure economic optimization. As it may be noticed, a pure environmental optimization introduces savings in the carbon dioxide emissions up to -20.6%; however, the total cost experiences a dramatic rise (+103.3%). A more realistic solution would be to establish a predefined trade-off value, between the two objective functions: the example provided in the figure consists in fixing the maximum increase in the cost to +25% with respect to the result of the economic optimization; in this way, reduction in the carbon footprint up to -12.1% would be possible.

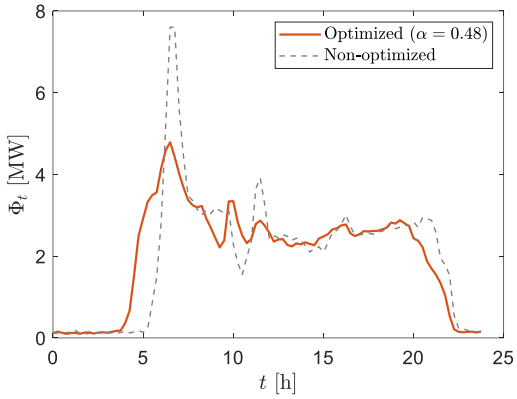

Figure 12. Evolution of the heat load at production plant during the day: comparison of the non-optimized case with the configuration obtained with an intermediate Pareto solution ($\alpha \approx 0.48$).

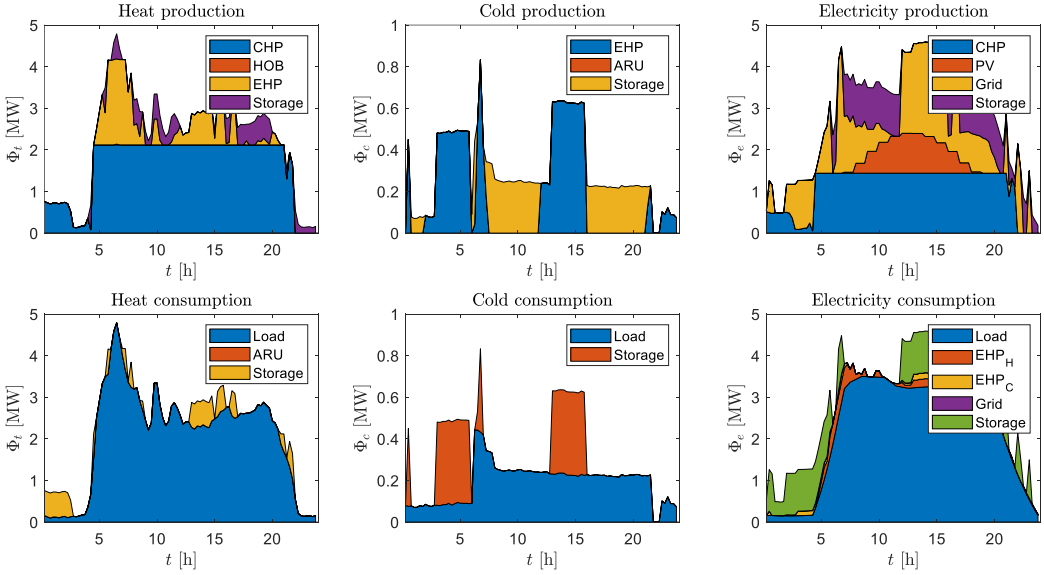

Figure 13. Optimized operation of the production plant for an intermediate Pareto solution ($\alpha \approx 0.48$).

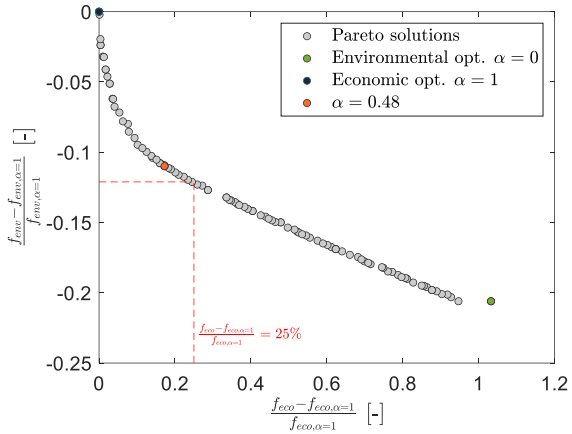

Figure 14. Result of the multi-objective optimization: variation of the Pareto solutions with respect to the results provided by the pure economic optimization.

5. CONCLUSIONS

In this paper, a global multi-objective optimization approach for the economic and environmental optimization of a complex multi-energy system was presented. The proposed tool allows the simultaneously optimization of production and demand, since it considers at the same time a) the possibility to perform demand-side management to shave the thermal peak, b) a network dynamic simulator (to correctly evaluate the thermal load at production plant level) and c) an optimizer for the smart management of the production technologies, including the storage units. The approach proposed allows quantifying the best operations for the production technologies and storages, along with the best set of time-shifting for the building thermal demand (i.e. best demand side management).

The proposed tool is based on a bi-level optimization structure: the upper-level deals with demand-side management and uses the genetic algorithm to find the best combination of anticipations to be applied to the thermal load of each customers; it also includes a physical model of the district heating network in order to properly reproduce the dynamic effects related with the anticipations; the lower-level optimization is devoted to the production optimization, which is obtained by means of a linear programming algorithm.

The economic optimization brought to a total cost of about 4700 €/day, while the corresponding carbon emissions would be approximately 25000 kg/day. In contrast, if the system is optimized with an environmental objective function, the production technologies are switched on according to different logics, allowing a reduction in the emissions up to 19800 kg/day; however, in this case, the daily cost increases reaching 9600 €. Due to the competing nature of the two objective functions, a multi-objective optimization was proposed to find the whole set of optimal solutions, represented in the Pareto front. This allows finding different optimal configurations of the system, depending on the trade-off established between the increase in the total cost and the carbon emissions reduction. Reduction in the carbon footprint of the system of about -12% would be possible if a 25% increase in the total expense is considered as acceptable (with respect to the result of a single-variable economic optimization).

REFERENCES

[1] S. Frederiksen and S. Werner, *District Heating and Cooling*. Studentlitteratur AB, 2013.

[2] S. Werner, "International review of district heating and cooling," *Energy*, vol. 137, pp. 617–631, 2017, doi: 10.1016/j.energy.2017.04.045.

[3] A. Lake, B. Rezaie, and S. Beyerlein, "Review of district heating and cooling systems for a sustainable future," *Renew. Sustain. Energy Rev.*, vol. 67, pp. 417–425, 2017, doi: 10.1016/j.rser.2016.09.061.

[4] P. Mancarella, "MES (multi-energy systems): An overview of concepts and evaluation models," *Energy*, vol. 65, pp. 1–17, 2014, doi: 10.1016/j.energy.2013.10.041.

[5] E. Fabrizio, V. Corrado, and M. Filippi, "A model to design and optimize multi-energy systems in buildings at the design concept stage," *Renew. Energy*, vol. 35, no. 3, pp. 644–655, 2010, doi: 10.1016/j.renene.2009.08.012.

[6] S. Mazzoni, S. Ooi, B. Nastasi, and A. Romagnoli, "Energy storage technologies as techno-economic parameters for master-planning and optimal dispatch in smart multi energy systems," *Appl. Energy*, vol. 254, no. June, p. 113682, 2019, doi: 10.1016/j.apenergy.2019.113682.

[7] R. Garmabdari, M. Moghimi, F. Yang, and J. Lu, "Multi-objective optimisation and planning of grid-connected cogeneration systems in presence of grid power fluctuations and energy storage dynamics," *Energy*, vol. 212, 2020, doi: 10.1016/j.energy.2020.118589.

[8] A. Bartolini, F. Carducci, C. B. Muñoz, and G. Comodi, "Energy storage and multi energy systems in local energy communities with high renewable energy penetration," *Renew. Energy*, vol. 159, pp. 595–609, 2020, doi: 10.1016/j.renene.2020.05.131.

[9] D. Sadeghi, A. Hesami Naghshbandy, and S. Bahramara, "Optimal sizing of hybrid renewable energy systems in presence of electric vehicles using multi-objective particle swarm optimization," *Energy*, vol. 209, p. 118471, 2020, doi: 10.1016/j.energy.2020.118471.

[10] F. Böing and A. Regett, *Hourly CO2 emission factors and marginal costs of energy carriers in future multi-energy systems*, vol. 12, no. 11. 2019.

[11] H. Lund, P. A. Østergaard, D. Connolly, and B. V. Mathiesen, "Smart energy and smart energy systems," *Energy*, vol. 137, pp. 556–565, 2017, doi: 10.1016/j.energy.2017.05.123.

[12] M. Sameti and F. Haghighat, "Optimization approaches in district heating and cooling thermal network," vol. 140, pp. 121–130, 2017.

[13] H. Wang, W. Yin, E. Abdollahi, R. Lahdelma, and W. Jiao, "Modelling and optimization of CHP based district heating system with renewable energy production and energy storage," vol. 159, pp. 401–421, 2015.

[14] A. Bischi *et al.*, "A detailed MILP optimization model for combined cooling, heat and power system operation planning," *Energy*, vol. 74, no. C, pp. 12–26, 2014, doi: 10.1016/j.energy.2014.02.042.

[15] A. Bischi *et al.*, "A rolling-horizon optimization algorithm for the long term operational scheduling of cogeneration systems," *Energy*, vol. 184, pp. 73–90, 2019, doi: 10.1016/j.energy.2017.12.022.

[16] A. Rieder, A. Christidis, and G. Tsatsaronis, "Multi criteria dynamic design optimization of a small scale distributed energy system," *Energy*, vol. 74, no. C, pp. 230–239, 2014, doi: 10.1016/j.energy.2014.06.007.

[17] D. Buoro, M. Casisi, A. De Nardi, P. Pinamonti, and M. Reini, "Multicriteria optimization of a distributed energy supply system for an industrial area," *Energy*, vol. 58, pp. 128–137, 2013, doi: 10.1016/j.energy.2012.12.003.
[18] K. M. Powell *et al.*, "Thermal energy storage to minimize cost and improve efficiency of a polygeneration district energy system in a real-time electricity market," *Energy*, vol. 113, pp. 52–63, 2016, doi: 10.1016/j.energy.2016.07.009.
[19] Y. Zhao, Y. Lu, C. Yan, and S. Wang, "MPC-based optimal scheduling of grid-connected low energy buildings with thermal energy storages," *Energy Build.*, vol. 86, pp. 415–426, 2015, doi: 10.1016/j.enbuild.2014.10.019.
[20] N. Deng *et al.*, "A MINLP model of optimal scheduling for a district heating and cooling system: A case study of an energy station in Tianjin," *Energy*, vol. 141, pp. 1750–1763, 2017, doi: 10.1016/j.energy.2017.10.130.
[21] P. Arcuri, P. Beraldi, G. Florio, and P. Fragiacomo, "Optimal design of a small size trigeneration plant in civil users: A MINLP (Mixed Integer Non Linear Programming Model)," *Energy*, vol. 80, pp. 628–641, 2015, doi: 10.1016/j.energy.2014.12.018.
[22] G. Schweiger *et al.*, "Active consumer participation in smart energy systems," *Energy Build.*, vol. 227, 2020, doi: 10.1016/j.enbuild.2020.110359.
[23] K. Kontu, P. Penttinen, J. Vimpari, and S. Junnila, "From partial optimization to overall system management – real-life smart heat load control in district heating systems," *Energy Build.*, vol. 204, 2019, doi: 10.1016/j.enbuild.2019.109481.
[24] E. Guelpa and V. Verda, "Demand response and other demand side management techniques for district heating: A review," *Energy*, vol. 219, p. 119440, 2021, doi: 10.1016/j.energy.2020.119440.
[25] F. Wernstedt, P. Davidsson, and C. Johansson, "Demand side management in district heating systems," *Proc. Int. Conf. Auton. Agents*, pp. 1383–1389, 2007, doi: 10.1145/1329125.1329454.
[26] P. Hietaharju and M. Ruusunen, "Peak Load Cutting in District Heating Network," *Proc. 9th EUROSIM Congr. Model. Simulation, EUROSIM 2016, 57th SIMS Conf. Simul. Model. SIMS 2016*, vol. 142, pp. 99–104, 2018, doi: 10.3384/ecp1714299.
[27] E. Guelpa, G. Mutani, V. Todeschi, and V. Verda, "Reduction of CO2 emissions in urban areas through optimal expansion of existing district heating networks," *J. Clean. Prod.*, vol. 204, pp. 117–129, 2018, doi: 10.1016/j.jclepro.2018.08.272.
[28] T. Sweetnam, C. Spataru, M. Barrett, and E. Carter, "Domestic demand-side response on district heating networks," *Build. Res. Inf.*, vol. 47, no. 4, pp. 330–343, 2019, doi: 10.1080/09613218.2018.1426314.
[29] S. Kärkkäinen, K. Sipilä, L. Pirvola, J. Esterinen, E. Eriksson, and S. Soikkeli, "Demand side management of the district heating systems," p. 104, 2003, [Online]. Available: http://www.vtt.fi/inf/pdf/.
[30] H. Cai, C. Ziras, S. You, R. Li, K. Honoré, and H. W. Bindner, "Demand side management in urban district heating networks," *Appl. Energy*, vol. 230, no. August, pp. 506–518, 2018, doi: 10.1016/j.apenergy.2018.08.105.
[31] E. Guelpa, S. Deputato, and V. Verda, "Thermal request optimization in district heating networks using a clustering approach," *Appl. Energy*, vol. 228, no. December 2017, pp. 608–617, 2018, doi: 10.1016/j.apenergy.2018.06.041.
[32] E. Guelpa and V. Verda, "Optimization of the Thermal Load Profile in District Heating Networks through 'virtual Storage' at Building Level," *Energy Procedia*, vol. 101, no. September, pp. 798–805, 2016, doi: 10.1016/j.egypro.2016.11.101.
[33] E. Guelpa and L. Marincioni, "Demand side management in district heating systems by innovative control," *Energy*, vol. 188, p. 116037, 2019, doi: 10.1016/j.energy.2019.116037.
[34] M. Capone, E. Guelpa, and V. Verda, "Optimal operation of district heating networks through demand response," *Int. J. Thermodyn.*, vol. 22, no. 1, pp. 35–43, 2019, doi: 10.5541/ijot.519101.
[35] D. Basciotti and R.-R. Schmidt, "Simulation Case Study on Load Shifting," *EuroHeat&Power*, vol. Vol. 10, no. January, 2013.
[36] E. Guelpa *et al.*, "Demand side management in district heating networks: A real application," *Energy*, vol. 182, pp. 433–442, 2019, doi: 10.1016/j.energy.2019.05.131.
[37] P. Ala-Kotila, T. Vainio, and J. Heinonen, "Demand Response in District Heating Market—Results of the Field Tests in Student Apartment Buildings," *Smart Cities*, vol. 3, no. 2, pp. 157–171, 2020, doi: 10.3390/smartcities3020009.
[38] M. Razmara, G. R. Bharati, D. Hanover, M. Shahbakhti, S. Paudyal, and R. D. Robinett, "Building-to-grid predictive power flow control for demand response and demand flexibility programs," *Appl. Energy*, vol. 203, pp. 128–141, 2017, doi: 10.1016/j.apenergy.2017.06.040.
[39] D. Rakipour and H. Barati, "Probabilistic optimization in operation of energy hub with participation of renewable energy resources and demand response," *Energy*, vol. 173, pp. 384–399, 2019, doi: 10.1016/j.energy.2019.02.021.
[40] J. Reynolds, M. W. Ahmad, Y. Rezgui, and J. L. Hippolyte, "Operational supply and demand optimisation of a multi-vector district energy system using artificial neural networks and a genetic algorithm," *Appl. Energy*, vol. 235, no. October 2018, pp. 699–713, 2019, doi: 10.1016/j.apenergy.2018.11.001.
[41] E. Guelpa, "Impact of network modelling in the analysis of district heating systems," *Energy*, vol. 213, 2020,

doi: 10.1016/j.energy.2020.118393.
[42] I. Gabrielaitiene, “Numerical simulation of a district heating system with emphases on transient temperature behaviour,” *8th Int. Conf. Environ. Eng. ICEE 2011*, no. January 2011, pp. 747–754, 2011.
[43] L. Wang, M. Lampe, P. Voll, Y. Yang, and A. Bardow, “Multi-objective superstructure-free synthesis and optimization of thermal power plants,” *Energy*, vol. 116, pp. 1104–1116, 2016, doi: 10.1016/j.energy.2016.10.007.
[44] F. Harary, *Graph theory*. New Delhi: Narosa Publishing, 1995.
[45] H. K. Versteeg and W. Malalasekera, *An introduction to computational fluid dynamics: The finite volume method*. Pearson Education Limited, 2017.
[46] A. Sciacovelli, V. Verda, and R. Borchiellini, *Numerical design of thermal systems*. CLUT Editrice, 2015.
[47] E. Guelpa, A. Sciacovelli, and V. Verda, “Thermo-fluid dynamic model of large district heating networks for the analysis of primary energy savings,” *Energy*, vol. 184, pp. 34–44, 2019, doi: 10.1016/j.energy.2017.07.177.
[48] ISPRA, “Fattore di emissione atmosferica di gas a effetto serra nel settore elettrico nazionale e nei principali Paesi Europei,” 2019.